

# Electronic State and Microenvironment Modulation of Metal Nanoparticles Stabilized by MOFs for Boosting Electrocatalytic Nitrogen Reduction

Lulu Wen, Kang Sun, Xiaoshuo Liu, Weijie Yang, Luyan Li, and Hai-Long Jiang\*

Modulation of the local electronic structure and microenvironment of catalytic metal sites plays a critical role in electrocatalysis, yet remains a grand challenge. Herein, PdCu nanoparticles with an electron rich state are encapsulated into a sulfonate functionalized metal-organic framework, UiO-66-SO<sub>3</sub>H (simply as UiO-S), and their microenvironment is further modulated by coating a hydrophobic polydimethylsiloxane (PDMS) layer, affording PdCu@UiO-S@PDMS. This resultant catalyst presents high activity toward the electrochemical nitrogen reduction reaction (NRR, Faraday efficiency: 13.16%, yield: 20.24 μg h<sup>-1</sup> mg<sub>cat.</sub><sup>-1</sup>), far superior to the corresponding counterparts. Experimental and theoretical results jointly demonstrate that the protonated and hydrophobic microenvironment supplies protons for the NRR yet suppresses the competitive hydrogen evolution reaction reaction, and electron-rich PdCu sites in PdCu@UiO-S@PDMS are favorable to formation of the N<sub>2</sub>H\* intermediate and reduce the energy barrier of NRR, thereby accounting for its good performance.

Amongst them, electrochemical N<sub>2</sub> reduction reaction (NRR) is emerging as a promising alternative strategy for the green synthesis of NH<sub>3</sub> under ambient conditions. However, due to the ultra-stable N≡N covalent triple bond as well as the competing hydrogen evolution reaction (HER) process, NRR suffers from sluggish reaction kinetics and unsatisfactory Faradaic efficiency (FE).<sup>[4]</sup> Therefore, it is highly desired to develop advanced catalysts that can inhibit the competitive HER, and promote the N<sub>2</sub> activation toward efficient electrocatalytic NRR.

Metal nanoparticles (NPs) have been recognized to be effective and intensively employed in electrocatalytic NRR at ambient conditions.<sup>[4c,d,5]</sup> The modulation of the electronic state of active metal sites and their surrounding microenvironment has been considered to play critical

roles in the catalytic performance.<sup>[6]</sup> Specifically, Pd NPs have been demonstrated to be potential NRR sites; unfortunately, molecular hydrogen is readily poisoned on the Pd surface due to its stronger binding to hydrogen adatoms than nitrogen.<sup>[5b]</sup> To address this issue, the integration of Cu with Pd to form PdCu alloys has been proven to be a feasible method. Recently, crystal phase engineering based on PdCu alloys was developed to modulate NRR performance, which proved the strong electronic interaction between Pd and Cu can not only weaken the Pd-H interaction to suppress HER process, but also boost NRR activity.<sup>[5c]</sup> Therefore, the introduction of the second metal Cu into Pd NPs would be a promising strategy to modulate the electronic state of Pd site for improved NRR.

In addition to surface electronic state regulation, the surface microenvironment modulation of metal NPs is usually achieved via the modification of diverse functional molecules on their surface,<sup>[7]</sup> such as surfactant, which is actually not favorable to the accessibility of active metal sites and the activity.<sup>[8]</sup> Alternatively, the encapsulation of metal NPs into porous materials with tailorable structures might be a judicious solution, because the metal NPs with naked surface and small sizes can be confined in pore spaces, and the interconnected pores make them easily accessible to the substrates. To impede the competitive HER process, the creation of hydrophobic microenvironment around metal sites will prevent the accessibility from water molecules to the catalytic sites.<sup>[9]</sup> However, NRR is a proton engaged process associated with gradual hydrogenation


## 1. Introduction

As an important chemical in industry, ammonia (NH<sub>3</sub>) has been widely used in energy carrier, fertilizer production, and fuel. To date, NH<sub>3</sub> production on an industrial scale is dominated via Haber-Bosch process at high temperature and pressure, suffering from energy intensive and environment unfriendly issues.<sup>[1]</sup> Therefore, it is significant to explore green and sustainable approaches for the NH<sub>3</sub> production. So far, many alternative strategies have been developed for artificial N<sub>2</sub> reduction technologies, including photocatalysis, electrocatalysis, etc.<sup>[2-4]</sup>

L. Wen, K. Sun, L. Li, H.-L. Jiang  
Department of Chemistry  
University of Science and Technology of China  
Hefei, Anhui 230026, P. R. China  
E-mail: jianglab@ustc.edu.cn

X. Liu, W. Yang  
School of Energy and Power Engineering  
North China Electric Power University  
Baoding, Hebei 071003, P. R. China

X. Liu  
School of Energy and Environment  
Southeast University  
Nanjing, Jiangsu 210096, P. R. China

 The ORCID identification number(s) for the author(s) of this article can be found under <https://doi.org/10.1002/adma.202210669>.

DOI: 10.1002/adma.202210669

steps, in which the participation of  $H^+$  is essential. To solve this contradiction, the introduction of protonated functional group, such as sulfonic acid ( $-SO_3H$ ), will provide proton (relay) for the NRR process, and the deprotonated  $-SO_3^-$  might be able to capture protons through the hydrophobic microenvironment.

To achieve the above design toward the incorporation of PdCu NPs and hydrophobic microenvironment with protonated functional groups, a class of crystalline porous materials, metal-organic frameworks (MOFs) and covalent-organic frameworks (COFs),<sup>[10]</sup> featuring high porosity and large surface area, as well as tailorable structures, would be promising candidates.<sup>[11]</sup> Recently, MOF based and COF based catalysts have shown unique advantages in electrocatalytic NRR, and provide an excellent platform to investigate the structure-property relationship at atomic level.<sup>[3e,9,12]</sup> Thanks to the porous structures, PdCu NPs can be well dispersed, stabilized, and accessed. Moreover, diverse functional groups can be dangled onto the pore walls of MOFs and COFs to modulate the microenvironment and local electronic state of guest metal sites, promoting the NRR performance. Therefore, the MOF or COF composites would be an ideal platform to investigate the influence of protonated and hydrophobic microenvironment modulation toward electrocatalytic NRR.

With these in mind, tiny PdCu NPs are incorporated into a representative MOF decorated with sulfonic acid group, UiO-66- $SO_3H$  ( $Zr_6O_4(OH)_4(BDC-SO_3H)_6$ , BDC = 1,4-benzenedicarboxylic acid; simply as UiO-S),<sup>[13]</sup> and further post-synthetic modification of polydimethylsiloxane (PDMS) affords the corresponding composite, denoted as PdCu@UiO-S@PDMS (Scheme 1). The electron transfer in PdCu NPs facilitates the conversion of  $N_2$  molecules, the protonated sulfonic acid microenvironment provides indispensable proton source for NRR, and the hydrophobic PDMS coating suppresses the contact of

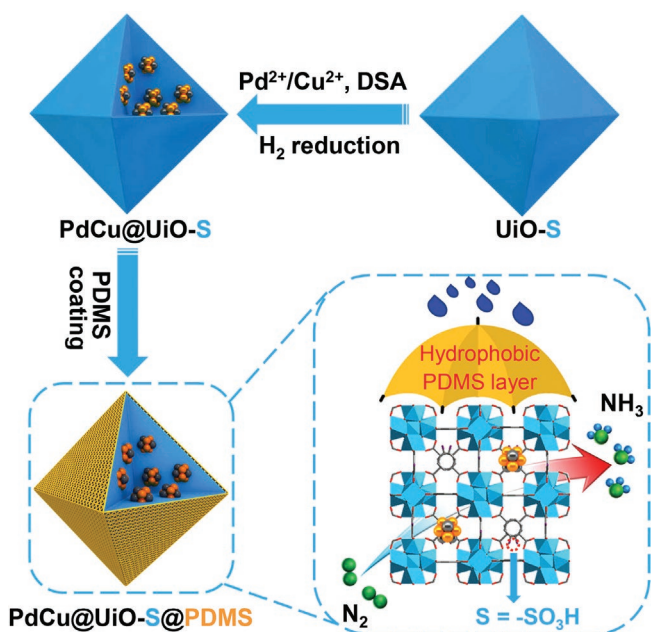
$H_2O$  with PdCu rather than preventing  $-SO_3^-$  to extract protons from the water. Therefore, an ideal microenvironment supplying protons yet suppressing competitive HER would be formed in PdCu@UiO-S@PDMS. As a result, the synergetic effect among the aforementioned factors in the composite catalyst cooperatively promotes the electrocatalytic NRR with good performance. Both experimental and theoretical calculations unveil that the presence of Cu atom increases the Pd electron density and induces an upshift of the d-band center of Pd atoms, thus benefiting to reduce the energy barrier of the NRR reaction, which are favorable to the catalytic process. This work provides a unique strategy to synergistically improve NRR by electron transfer coupled with microenvironmental modulation by MOF/COF materials.

## 2. Results and Discussion

### 2.1. Synthesis and Characterization

The UiO-66- $SO_3H$  (simply as UiO-S for clarity) can be activated upon heating to incorporate metal NPs into its pore space. To prevent the formation of metal NPs on the MOF external surface and avoid their aggregation, a double solvent approach synthetic strategy was adopted to rationally introduce Pd and PdCu NPs to afford Pd@UiO-S and PdCu@UiO-S, respectively (see the Experimental Section).<sup>[14]</sup> Given the hydrophilic cages in the MOF, the quantitative metal precursor aqueous solution can be fully introduced via the capillary force and hydrophilic interaction to yield metal precursor@UiO-S, which was further reduced by  $H_2$  to generate metal NPs confined in the MOF. The hydrophobic PDMS layer was further coated onto the PdCu@UiO-S composite by a simple vapor deposition method at 230 °C,<sup>[15]</sup> producing PdCu@UiO-S@PDMS.

Powder X-ray diffraction (XRD) patterns demonstrate the integrity of structure and crystallinity of the MOF after the reduction and post-synthetic PDMS modification (Figure S1–S3, Supporting Information). No identifiable diffraction peaks for Pd/Cu NPs in the composites indicate that metal NPs could be very small. Scanning electron microscopy (SEM) observation shows that PdCu@UiO-S@PDMS has a particle-stacking shape with average sizes of ca. 120 nm (Figure 1a). The related control samples present similar morphologies and sizes (Figure S4–S7). The transmission electron microscopy (TEM) images display that the outer surface of the catalyst is obviously coated with a thin layer of PDMS of  $\approx 1$  nm, and the coating of the hydrophobic PDMS layer does not affect the morphology and size (Figure 1b,c; Figure S8, Supporting Information). There are no observable Pd or PdCu NPs in the TEM images, which suggests that they are in very small sizes, in line with the above powder XRD results. Nitrogen adsorption measurements indicate that PdCu@UiO-S and PdCu@UiO-S@PDMS possess similar Brunauer-Emmett-Teller surface area, and the slight decrease in surface area compared to parent UiO-S is ascribed to the mass occupation of PdCu NPs (Figure S9). The high surface area of PdCu@UiO-S@PDMS reveals that the thin PDMS coating layer is permeable and does not impede the transportation of  $N_2$  molecules. Elemental mapping results support the even dispersion of Pd, Cu, and Zr in the sample (Figure 1d).



**Scheme 1.** Schematic illustration for the stepwise synthesis of PdCu@UiO-S@PDMS with significant functional components/units for improving NRR being highlighted.

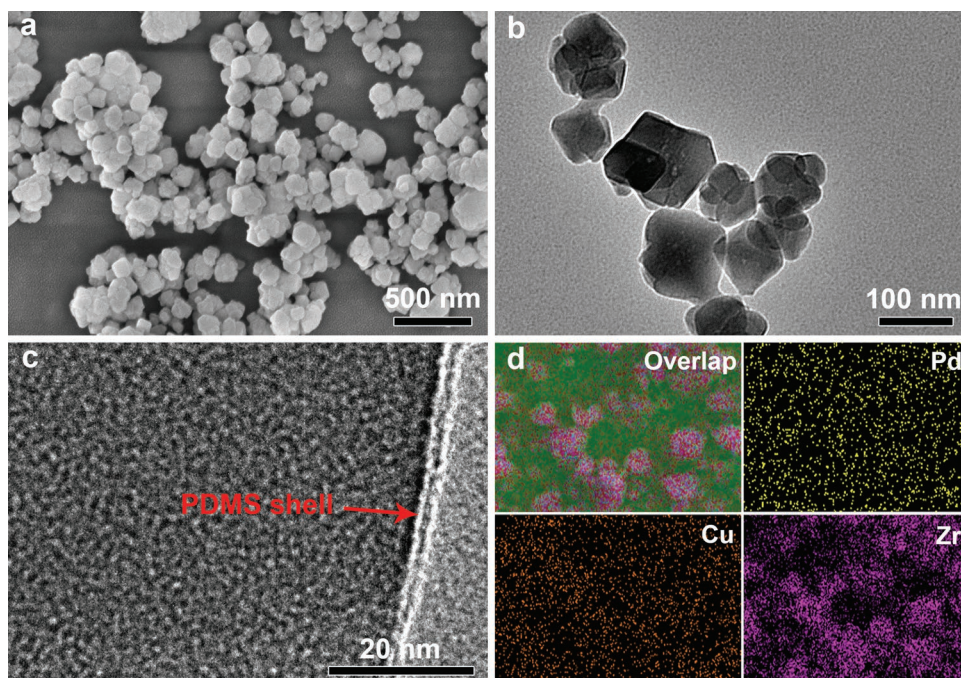


**Figure 1.** a) SEM image, and b) low- and c) high-magnification TEM images, as well as d) elemental mapping images for PdCu@UiO-S@PDMS.

In addition, the molar ratio of Pd and Cu is adjusted to  $\approx 9:1$  while fixing their total amount at  $\approx 2.0$  wt.% in PdCu@UiO-S@PDMS, as evaluated by the inductively coupled plasma atomic emission spectroscopy (Table S1).

## 2.2. Electrochemical NRR Performance

Linear sweep voltammetry curves were recorded under  $N_2$  and Ar saturated electrolytes, respectively. The higher current density at a lower potential in  $N_2$  atmosphere implies potential NRR activity (Figure S10). Encouraged by this, the electrocatalytic NRR experiments and the corresponding electrochemical tests were conducted in a two compartment electrochemical cell in 0.1 M HCl electrolyte, and all potentials were converted to the RHE scale. The concentration of the produced  $NH_3$  was quantified by the indophenol blue methods spectrophotometrically (Figure S11), and the possible  $N_2H_4$  (byproduct) was determined by the Watt and Chrisp method (Figure S12).<sup>[16]</sup> Time dependent current density curves of given potentials in  $N_2$ -saturated electrolyte indicate that the current density increases in order from -0.05 to -0.45 V versus RHE (Figure S13). The UV-vis absorption spectra of the electrolytes stained with the indophenol indicator at a series of potentials after 2 h of electrolysis are collected to quantify the produced  $NH_3$  (Figure S14). By comparison of the collected data, the largest  $NH_3$  yield of  $20.24 \mu g h^{-1} mg_{cat.}^{-1}$  and the highest FE of 13.16% are achieved by PdCu@UiO-S@PDMS at -0.25 V with current density of  $\approx 0.142 mA cm^{-2}$  under ambient conditions (Figure 2a). Meanwhile, the amount of  $NH_3$  increases with increasing time, indicating the continuous catalytic process (Figure S15). When a more negative potential is applied, the PDMS coating still presents hydrophobic characteristics indicating the stability

of PDMS overlayer (Figure S16 and S17). The decreased  $NH_3$  yield and FE are probably caused by the gradually enhanced competitive HER.<sup>[2b]</sup> It should be noted that the current density decreases with increasing the particle size of MOF, which is attributed to the higher internal electrical resistance in large MOF (Figure S18 and S19). The obtained activity is comparable and even superior to those of reported Pd based and MOF/COF based NRR electrocatalysts under similar conditions (Table S2; Figure S3, Supporting Information). Furthermore, the concentration of  $NH_3$  has also been quantified by nuclear magnetic resonance (NMR) spectroscopy and the signal integration-concentration linear relation is obtained (Figure S20). The concentration of  $NH_4^+$  is calculated to be  $20.92 \mu g h^{-1} mg_{cat.}^{-1}$ , which is consistent with the above UV-vis result ( $20.24 \mu g h^{-1} mg_{cat.}^{-1}$ ), unambiguously evidencing the efficient  $N_2$  reduction to  $NH_3$  over PdCu@UiO-S@PDMS (Figure S20b, Supporting Information). Moreover, the byproduct of  $N_2H_4$  is not detectable at all potentials investigated (Figure S21), suggesting the excellent selectivity to  $NH_3$  in the presence of PdCu@UiO-S@PDMS catalyst.

Control catalysts have been fabricated to identify the key components in the optimized structure (Figure 2b; Figure S22, Supporting Information). In the absence of metal NPs, the UiO-S@PDMS shows very low  $NH_3$  yield and FE, suggesting that PdCu NPs are necessary and should be active sites. The apparently higher NRR activity of PdCu@UiO-S@PDMS than that of Pd@UiO-S@PDMS reveals that Cu dopant plays positive influence in the NRR process,<sup>[5b,c]</sup> of which the optimized Cu/(Pd+Cu) molar ratio is  $\approx 10\%$  (Figure S23), affording the best activity and being defined as the default value. To further confirm the positive effect of Cu on NRR, electrochemical impedance spectroscopy (EIS) and electrochemical active surface area tests are performed (Figure S24–S26), indicating the

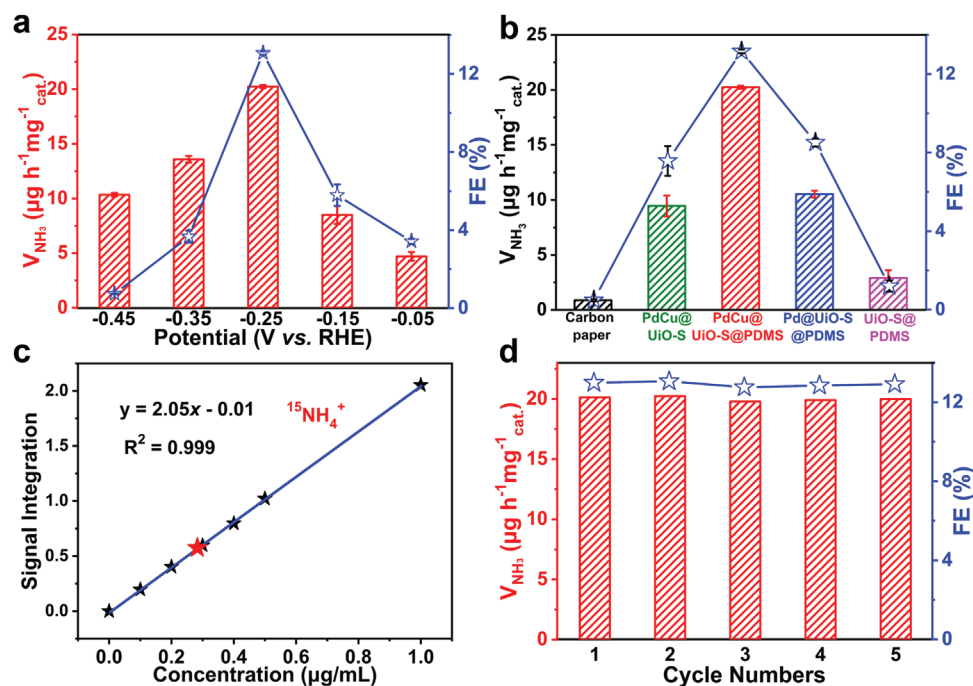


**Figure 2.** The  $\text{NH}_3$  yield rate and FE of a) PdCu@UiO-S@PDMS at various potentials, and b) the control catalysts, including carbon paper, PdCu@UiO-S, PdCu@UiO-S@PDMS, PdCu@UiO@PDMS, and UiO-S@PDMS at -0.25 V versus RHE. c) The  $^1\text{H}$  NMR calibration curve of  $^{15}\text{NH}_4^+$ . The red asterisk indicates the  $^{15}\text{NRR}$  product over PdCu@UiO-S@PDMS at -0.25 V in 0.1 M HCl. d) The FE and  $\text{NH}_3$  yield rate during the recycling test under the potential of -0.25 V versus RHE.

smaller charge transfer resistance and larger active surface area in PdCu counterpart than that of Pd counterpart. Moreover, PdCu@UiO@PDMS, in which UiO-66- $\text{SO}_3\text{H}$  is replaced with UiO-66, gives much reduced activity, indicating the protonated microenvironment created by  $-\text{SO}_3\text{H}$  group is of great importance in electrocatalytic NRR. In addition, the contact angles of UiO-S and PdCu@UiO-S are  $\approx 2.2^\circ$ , showing super hydrophilic properties. Upon coating PDMS, the PdCu@UiO-S@PDMS gives a contact angle of  $137.3^\circ$  and strong hydrophobic feature (Figure S16). This hydrophobic PDMS coating layer plays a critical role in the inhibition of competitive HER, as can be supported by the significantly lower limiting current of PdCu@UiO-S@PDMS than that of PdCu@UiO-S catalyst (Figure S27). Meanwhile, the apparent current response indicates that PDMS will not completely repulse all protons, affording a moderate proton environment that might be suitable for NRR.

To verify whether the  $\text{NH}_3$  detected is only produced from electrocatalytic  $\text{N}_2$  reduction over PdCu@UiO-S@PDMS, control experiments have been carried out in  $\text{N}_2$  saturated solution under an open circuit potential and Ar saturated solution at -0.25 V for 2 h. The corresponding UV-vis absorption spectra suggest that almost no  $\text{NH}_3$  generation for the above two situations (Figure S28). To further examine the source of  $\text{NH}_3$ , the isotope labeling experiments were conducted. The  $^1\text{H}$  NMR spectra of the standard samples display triplet and duplet coupling for  $^{14}\text{NH}_4^+$  and  $^{15}\text{NH}_4^+$ , respectively (Figure S29).<sup>[4d]</sup> By using  $^{15}\text{N}_2$  as the feed gas for the electrolytic reaction at -0.25 V versus RHE, only the duplet coupling signal associated with the standard  $^{15}\text{NH}_4^+$  can be identified (Figure S30). The signal integration of the  $^{15}\text{N}$  duplet coupling corresponds to the  $^{15}\text{NH}_4^+$  concentration of  $21.38 \mu\text{g h}^{-1} \text{mg}_{\text{cat.}}^{-1}$  (Figure 2c),

unambiguously manifesting that the  $\text{NH}_3$  is indeed produced from electrocatalytic  $\text{N}_2$  reduction.

Stability is another critical parameter to assess NRR performance for practical applications. The stability of PdCu@UiO-S@PDMS was evaluated by five consecutive runs of electrocatalysis at -0.25 V (Figure 2d), during which both FE and  $\text{NH}_3$  yields give very slight fluctuations, indicating the excellent stability in electrochemical NRR. Moreover, the electrocatalytic NRR over PdCu@UiO-S@PDMS at -0.25 V under a sustained  $\text{N}_2$  gas bubbling flow for 20 h exhibits almost no variation of the current density (Figure S31), further demonstrating its good stability. After long term NRR electrocatalysis over PdCu@UiO-S@PDMS, powder XRD results present almost negligible change in the crystalline phase, and the SEM, TEM, and elemental mapping images indicate that its microstructure is maintained (Figure S32). The leaching of  $\text{Zr}^{4+}$ ,  $\text{Cu}^{2+}$  and  $\text{Pd}^{4+}$  in electrolyte are measured and the obtained results generally support the catalyst stability (Table S4). X-ray photoelectron spectroscopy (XPS) spectra reveal that no significant peak shift or oxidation state change for Pd, Cu, and S can be observed after the NRR process (Figure S33 and S34). All these results support that this catalyst remains stable under the electrocatalytic NRR conditions. It should be noted that the PDMS does not obviously enhance the chemical stability of PdCu@UiO-S probably due to the originally high stability of UiO-type MOFs in acidic solution (Figure S35).

### 2.3. Reaction Mechanism

To understand the reason behind the high NRR activity of PdCu@UiO-S@PDMS, XPS is adopted to characterize

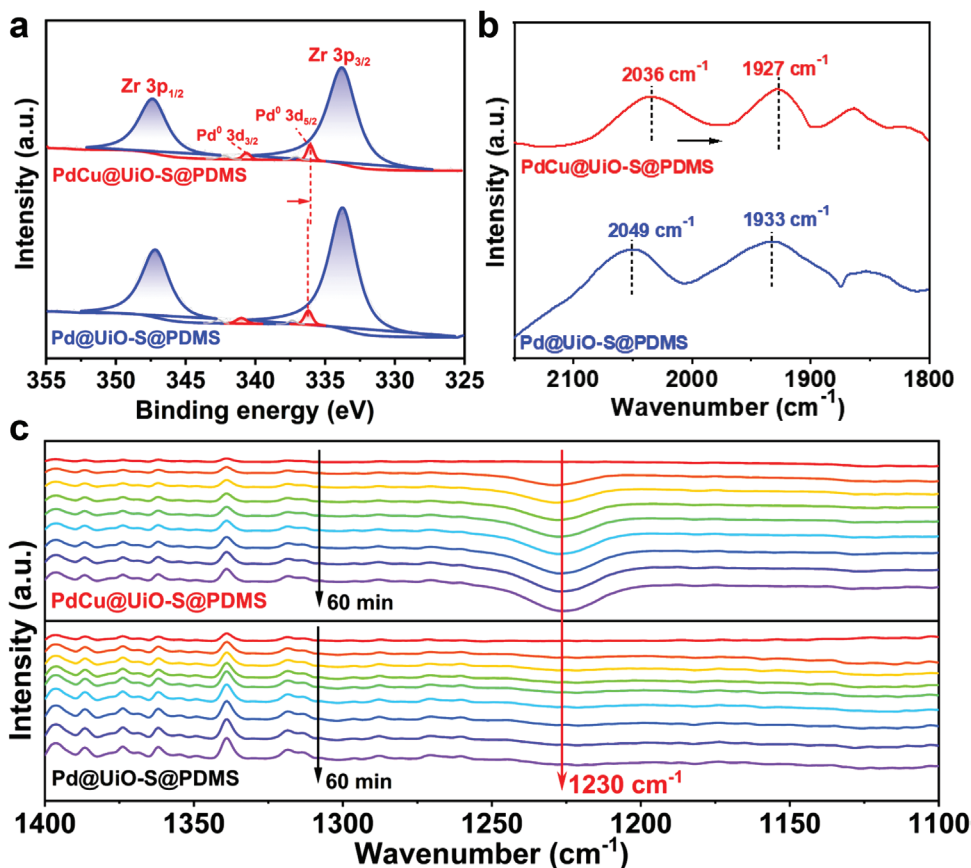


**Figure 3.** a) The Pd 3d XPS spectra and b) CO-DRIFT spectra for PdCu@UiO-S@PDMS and Pd@UiO-S@PDMS. In situ FT-IR spectra of c) Pd@UiO-S@PDMS and PdCu@UiO-S@PDMS during the electrocatalytic reaction at  $-0.25$  V versus RHE for 60 min.

its surface electronic structure (Figure 3a). The peak of Pd  $3d_{5/2}$  in PdCu@UiO-S@PDMS is located at 336.0 eV, presenting a slight shift to lower binding energy upon alloying with Cu, as compared with that at 336.3 eV for Pd@UiO-S@PDMS.<sup>[17]</sup> The binding energy shift reflects that the Pd surface in PdCu@UiO-S@PDMS becomes electron-rich and presents charge redistribution effect between Pd and Cu.<sup>[5b]</sup> The spectra of Cu  $2p_{3/2}$  can be split into two peaks, related to Cu<sup>0</sup> (932.6 eV, 952.6 eV) and Cu<sup>2+</sup> (934.6 eV, 953.8 eV) (Figure S33b, Supporting Information). The partial oxidation of Cu<sup>0</sup> observed, which is commonly reported,<sup>[5d]</sup> might be due to the oxidation by air exposure. The clear signal for Si 2p after PDMS coating demonstrates the successful surface modification for PdCu@UiO-S (Figure S36).<sup>[15]</sup> In addition, to further verify the electronic state of Pd, the diffuse reflectance infrared Fourier transform (DRIFT) spectra of CO adsorption are collected (Figure 3b). The Pd@UiO-S@PDMS gives the CO adsorption peaks at 2049  $\text{cm}^{-1}$  and 1933  $\text{cm}^{-1}$ , which are associated with the linearly adsorbed and bridge-bound CO, respectively.<sup>[7a]</sup> Upon integrating Cu with Pd, the main CO adsorption peaks of PdCu@UiO-S@PDMS exhibit a blue shift to a lower wavenumber, indicating that the electron donating effect of Cu makes Pd surface rich in electrons, giving rise to increased N<sub>2</sub> adsorption and enhanced NRR activity.

In situ Fourier transform infrared (FT-IR) spectra are adopted to compare the activity of electrocatalytic NRR over Pd@UiO-S@PDMS and PdCu@UiO-S@PDMS at  $-0.25$  V versus RHE (Figure 3c). Along with prolonged reaction time, the characteristic peak of NH<sub>3</sub> for Pd@UiO-S@PDMS at wavenumber of 1230  $\text{cm}^{-1}$  does not change significantly, while that for PdCu@UiO-S@PDMS gradually increases.<sup>[18]</sup> The result further supports that the increased Pd electronic density by incorporating Cu species is beneficial to enhanced activity in the NRR.

Density functional theory (DFT) calculations unveil the mechanism behind the superior activity of PdCu-based catalysts to the Pd based one. The Gibbs free energy ( $\Delta G$ ) variation along the coordinate of the reaction paths for Pd@UiO-S@PDMS and PdCu@UiO-S@PDMS is displayed (Figure 4a, see the detailed configurations in Figure S37). It can be seen that the formation of N<sub>2</sub>H\* is the rate determining step (RDS) for both alternating pathway and distal pathway, where PdCu@UiO-S@PDMS displays a much lower energy barrier (0.40 eV) for RDS than that of Pd@UiO-S@PDMS (1.16 eV). Even though the last desorption of NH<sub>3</sub>\* is endothermic, the protonation of NH<sub>3</sub>\* would form NH<sub>4</sub><sup>+</sup> in solution which is considered as a favorable step.<sup>[19]</sup> This result is consistent with superior experimental NRR activity of the PdCu@UiO-S@PDMS to the Pd counterpart. To rationalize the lower RDS energy barrier of the PdCu counterparts,

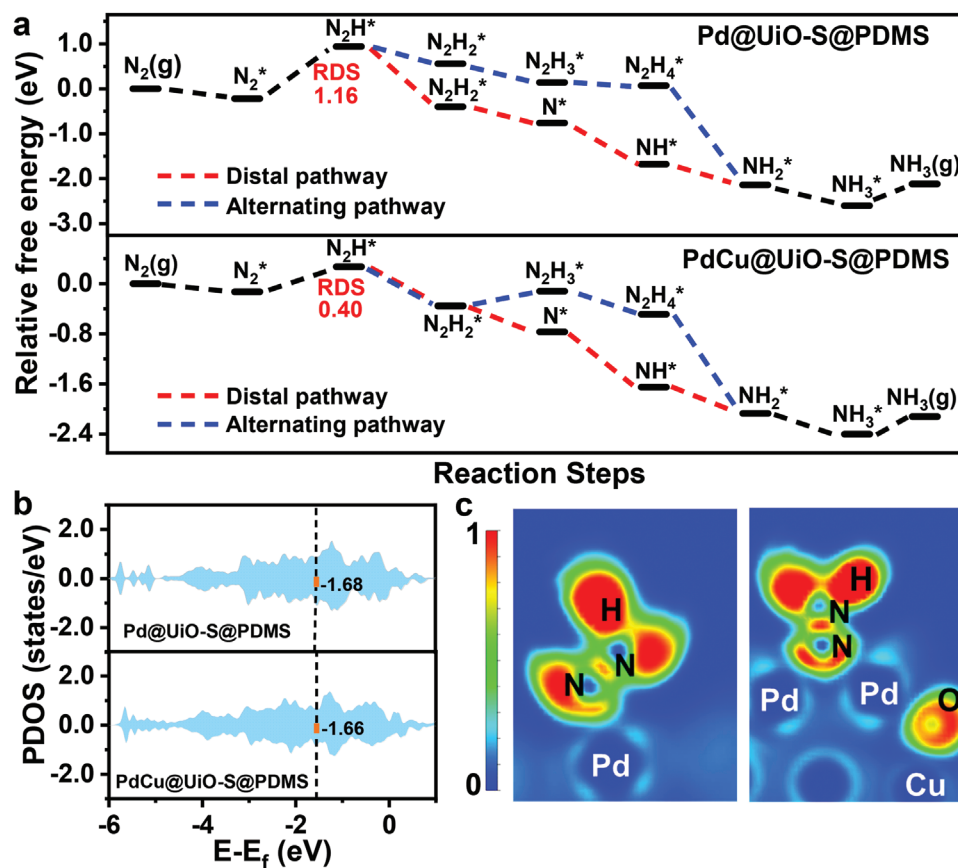


**Figure 4.** a) The energy variations of NRR process along reaction path of Pd@UiO-S@PDMS and PdCu@UiO-S@PDMS. b) The partial density of states and d-band center values of Pd atom on Pd@UiO-S@PDMS and PdCu@UiO-S@PDMS. c) The ELF of \*N<sub>2</sub>H absorbed on Pd@UiO-S@PDMS and PdCu@UiO-S@PDMS, respectively.

the d-band center of Pd reflecting the binding strength between N<sub>2</sub>H\* and active sites has been investigated.<sup>[5c]</sup> When the d-band center of catalytic sites is shifted up to the Fermi level, there will be a stronger bond strength between intermediates and catalytic sites as well as accelerated electron transfer. Compared to the Pd NPs, it can be seen that the introduction of Cu will lead to an upshift of the d-band center of Pd sites (Figure 4b), which indicates more occupied d-band electrons on PdCu counterpart. Consequently, the electron localization function (ELF) indicates that there is a greater degree of electron overlap in PdCu@UiO-S@PDMS, which manifests a stronger Pd-N interaction between N<sub>2</sub>H\* and Pd sites (Figure 4c). Bader charge analysis suggests that the upshift of d-band center and enhanced interaction arise from the electron donating effect of Cu (1.40 e), which is consistent with the above XPS and CO-DRIFT results.

### 3. Conclusion

In summary, tiny PdCu NPs have been encapsulated into a representative MOF, UiO-66-SO<sub>3</sub>H, followed by post-synthetic coating of PDMS layer, to afford PdCu@UiO-S@PDMS composite. This catalyst not only optimizes the electronic state of Pd active sites by alloying with Cu species, which reduces the energy barriers of RDS toward N<sub>2</sub> activation, but also

achieves unique protonated and moderate hydrophobic micro-environment modulation by grafting the -SO<sub>3</sub>H group on the MOF skeleton and coating PDMS layer, respectively. As a result, PdCu@UiO-S@PDMS exhibits high NRR activity up to 20.24 μg h<sup>-1</sup> mg<sub>cat.</sub><sup>-1</sup> with FE of 13.16% and stability in the electrocatalytic NRR, far surpassing the corresponding counterparts. The results highlight the integration of electron rich metal sites with protonated and hydrophobic microenvironment is crucial to enhance NRR activity and the suppression of the HER. DFT calculations indicate that the impressive activity of PdCu@UiO-S@PDMS is mainly attributed to the synergistic effect in the composite, which enriches the d-band electron density in Pd, and thereby giving rise to enhanced Pd-N interaction between N<sub>2</sub>H\* intermediate and Pd sites. This work offers a guideline to the integration of diverse functional species into a single composite based on advanced MOF platform for excellent catalysis, but also provides significant inspiration on promoting electrocatalysis by modulating microenvironment around catalytic metal centers.

### Supporting Information

Supporting Information is available from the Wiley Online Library or from the author.

## Acknowledgements

L.W., K.S., and X.L. contributed equally to this work. This work was supported by the National Key Research and Development Program of China (2021YFA1500402), the National Natural Science Foundation of China (22161142001, U22A20401, 21725101, and 52201232, and the Fundamental Research Funds for the Central Universities (WK3450000007 and WK2060000038).

## Conflict of Interest

The authors declare no conflict of interest.

## Data Availability Statement

The data that support the findings of this study are available from the corresponding author upon reasonable request.

## Keywords

electrocatalysis, electronic state, metal-organic frameworks, microenvironment modulation, N<sub>2</sub> reduction

Received: November 16, 2022

Revised: January 20, 2023

Published online: March 4, 2023

- [1] A. J. Martín, T. Shinagawa, J. Pérez-Ramírez, *Chem* **2019**, *5*, 263.
- [2] a) X. Cui, C. Tang, Q. Zhang, *Adv. Energy Mater.* **2018**, *8*, 1800369; b) W. Guo, K. Zhang, Z. Liang, R. Zou, Q. Xu, *Chem. Soc. Rev.* **2019**, *48*, 5658; c) C. Tang, S.-Z. Qiao, *Chem. Soc. Rev.* **2019**, *48*, 3166; d) X. Zhao, G. Hu, G.-F. Chen, H. Zhang, S. Zhang, H. Wang, *Adv. Mater.* **2021**, *33*, 2007650; e) G. Qing, R. Ghazfar, S. T. Jackowski, F. Habibzadeh, M. M. Ashtiani, C.-P. Chen, M. R. Smith III, T. W. Hamann, *Chem. Rev.* **2020**, *120*, 5437.
- [3] a) J. Yang, Y. Guo, W. Lu, R. Jiang, J. Wang, *Adv. Mater.* **2018**, *30*, 1802227; b) T.-N. Ye, S.-W. Park, Y. Lu, J. Li, M. Sasase, M. Kitano, T. Tada, H. Hosono, *Nature* **2020**, *583*, 391; c) P. Garrido-Barros, J. Derosa, M. J. Chalkley, J. C. Peters, *Nature* **2022**, *609*, 71; d) Y. Zhao, Y. Zhao, R. Shi, B. Wang, G. I. N. Waterhouse, L.-Z. Wu, C.-H. Tung, T. Zhang, *Adv. Mater.* **2019**, *31*, 1806482; e) B. Guo, X. Cheng, Y. Tang, W. Guo, S. Deng, L. Wu, X. Fu, *Angew. Chem. Int. Ed.* **2022**, *61*, 202117244.
- [4] a) C. Lv, Y. Qian, C. Yan, Y. Ding, Y. Liu, G. Chen, G. Yu, *Angew. Chem. Int. Ed.* **2018**, *57*, 10246; b) H.-L. Du, M. Chatti, R. Y. Hodgetts, P. V. Cherepanov, C. K. Nguyen, K. Matuszek, D. R. MacFarlane, A. N. Simonov, *Nature* **2022**, *609*, 722; c) Y. Wang, W. Zhou, R. Jia, Y. Yu, B. Zhang, *Angew. Chem. Int. Ed.* **2020**, *59*, 5350; d) Y.-C. Hao, Y. Guo, L.-W. Chen, M. Shu, X.-Y. Wang, T.-A. Bu, W.-Y. Gao, N. Zhang, X. Su, X. Feng, J.-W. Zhou, B. Wang, C.-W. Hu, A.-X. Yin, R. Si, Y.-W. Zhang, C.-H. Yan, *Nat. Catal.* **2019**, *2*, 448; e) R. Zhang, L. Jiao, W. Yang, G. Wan, H.-L. Jiang, *J. Mater. Chem. A* **2019**, *7*, 26371; f) S. Zhao, X. Lu, L. Wang, J. Gale, R. Amal, *Adv. Mater.* **2019**, *31*, 1805367; g) F. Wang, L. Mao, H. Xie, J. Mao, *Small Struct.* **2021**, *2*, 2000075.
- [5] a) M. I. Ahmed, C. Liu, Y. Zhao, W. Ren, X. Chen, S. Chen, C. Zhao, *Angew. Chem. Int. Ed.* **2020**, *59*, 21465; b) M.-M. Shi, D. Bao, S.-J. Li, B.-R. Wulan, J.-M. Yan, Q. Jiang, *Adv. Energy Mater.* **2018**, *8*, 1800124; c) W. Tong, B. Huang, P. Wang, L. Li, Q. Shao, X. Huang, *Angew. Chem. Int. Ed.* **2020**, *59*, 2649; d) C. Kim, J.-Y. Song, C. Choi, J. P. Ha, W. Lee, Y. T. Nam, D. Lee, G. Kim, I. Gereige, W.-B. Jung, H. Lee, Y. Jung, H. Jeong, H.-T. Jung, *Adv. Mater.* **2022**, *34*, 2205270.
- [6] a) L. Jiao, J. Wang, H.-L. Jiang, *Acc. Mater. Res.* **2021**, *2*, 327; b) X. Li, L. Liu, X. Ren, J. Gao, Y. Huang, B. Liu, *Sci. Adv.* **2020**, *6*, 6833; c) X. Wang, S. Qiu, J. Feng, Y. Tong, F. Zhou, Q. Li, L. Song, S. Chen, K.-H. Wu, P. Su, S. Ye, F. Hou, S. X. Dou, H. K. Liu, G. Q. (Max) Lu, C. Sun, J. Liu, J. Liang, *Adv. Mater.* **2020**, *32*, 2004382; d) Y. Wang, A. Xu, Z. Wang, L. Huang, J. Li, F. Li, J. Wicks, M. Luo, D.-H. Nam, C.-S. Tan, Y. Ding, J. Wu, Y. Lum, C.-T. Dinh, D. Sinton, G. Zheng, E. H. Sargent, *J. Am. Chem. Soc.* **2020**, *142*, 5702.
- [7] a) L. Li, Z. Li, W. Yang, Y. Huang, G. Huang, Q. Guan, Y. Dong, J. Lu, S.-H. Yu, H.-L. Jiang, *Chem* **2021**, *7*, 686; b) D. Chen, W. Yang, L. Jiao, L. Li, S.-H. Yu, H.-L. Jiang, *Adv. Mater.* **2020**, *32*, 2000041.
- [8] M. Xu, D. Li, K. Sun, L. Jiao, C. Xie, C. Ding, H.-L. Jiang, *Angew. Chem. Int. Ed.* **2021**, *60*, 16372.
- [9] a) Y. Yang, S. Q. Wang, H. Wen, T. Ye, J. Chen, C. P. Li, M. Du, *Angew. Chem. Int. Ed.* **2019**, *58*, 15362; b) S. Liu, T. Qian, M. Wang, H. Ji, X. Shen, C. Wang, C. Yan, *Nat. Catal.* **2021**, *4*, 322.
- [10] a) H. Furukawa, K. E. Cordova, M. O'Keeffe, O. M. Yaghi, *Science* **2013**, *341*, 1230444; b) H.-C. Zhou, S. Kitagawa, *Chem. Soc. Rev.* **2014**, *43*, 5415; c) T. Islamoglu, S. Goswami, Z. Li, A. J. Howarth, O. K. Farha, J. T. Hupp, *Acc. Chem. Res.* **2017**, *50*, 805; d) H. Li, L. Li, R.-B. Lin, W. Zhou, Z. Zhang, S. Xiang, B. Chen, *Energy Chem* **2019**, *1*, 100006; e) C. Li, S. Li, T. Hang, F. Guo, X.-D. Zhu, T.-F. Liu, *Small Struct.* **2022**, *3*, 2100071; f) Q.-G. Zhai, X. Bu, X. Zhao, D.-S. Li, P. Feng, *Acc. Chem. Res.* **2017**, *50*, 407; g) K. Chen, X.-L. Wang, W. Hu, Q. Kong, H. Pang, Q. Xu, *Small Struct.* **2022**, *3*, 2100200.
- [11] a) Q. Yang, Q. Xu, H.-L. Jiang, *Chem. Soc. Rev.* **2017**, *46*, 4774; b) Y. Zhao, N. Kornienko, Z. Liu, C. Zhu, S. Asahina, T.-R. Kuo, W. Bao, C. Xie, A. Hexemer, O. Terasaki, P. Yang, O. M. Yaghi, *J. Am. Chem. Soc.* **2015**, *137*, 2199; c) X. Li, T. W. Goh, L. Li, C. Xiao, Z. Guo, X. Zeng, W. Huang, *ACS Catal.* **2016**, *6*, 3461; d) H. Liu, L. Chang, C. Bai, L. Chen, R. Lu, Y. Li, *Angew. Chem. Int. Ed.* **2016**, *55*, 5019; e) J.-D. Xiao, L. Han, J. Luo, S.-H. Yu, H.-L. Jiang, *Angew. Chem. Int. Ed.* **2018**, *57*, 1103; f) G. Li, S. Zhao, Y. Zhang, Z. Tang, *Adv. Mater.* **2018**, *30*, 1800702; g) X. Zhang, J. Han, J. Guo, Z. Tang, *Small Struct.* **2021**, *2*, 2000141; h) Y. Jiang, Y. Yu, X. Zhang, M. Weinert, X. Song, J. Ai, L. Han, H. Fei, *Angew. Chem. Int. Ed.* **2021**, *60*, 17388; i) J. Liu, Y.-Z. Fan, K. Zhang, L. Zhang, C.-Y. Su, *J. Am. Chem. Soc.* **2020**, *142*, 14548; j) C. Fang, L. Liu, J. Weng, S. Zhang, X. Zhang, Z. Ren, Y. Shen, F. Meng, B. Zheng, S. Li, J. Wu, W. Shi, S. Lee, W. Zhang, F. Huo, *Angew. Chem. Int. Ed.* **2021**, *60*, 976.
- [12] a) S. Liu, M. Wang, T. Qian, H. Ji, J. Liu, C. Yan, *Nat. Commun.* **2019**, *10*, 3898; b) H. Zhong, M. Wang, M. Ghorbani-Asl, J. Zhang, K. H. Ly, Z. Liao, G. Chen, Y. Wei, B. P. Biswal, E. Zschech, I. M. Weidinger, A. V. Krashennikov, R. Dong, X. Feng, *J. Am. Chem. Soc.* **2021**, *143*, 19992.
- [13] K. M. Choi, K. Na, G. A. Somorjai, O. M. Yaghi, *J. Am. Chem. Soc.* **2015**, *137*, 7810.
- [14] a) Q.-L. Zhu, J. Li, Q. Xu, *J. Am. Chem. Soc.* **2013**, *135*, 10210; b) Y.-Z. Chen, B. Gu, T. Uchida, J. Liu, X. Liu, B.-J. Ye, Q. Xu, H.-L. Jiang, *Nat. Commun.* **2019**, *10*, 3462.
- [15] W. Zhang, Y. Hu, J. Ge, H.-L. Jiang, S.-H. Yu, *J. Am. Chem. Soc.* **2014**, *136*, 16978.
- [16] a) J. Zheng, Y. Lyu, M. Qiao, J. P. Veder, R. D. Marco, J. Bradley, R. Wang, Y. Li, A. Huang, S. P. Jiang, S. Wang, *Angew. Chem. Int. Ed.* **2019**, *58*, 18604; b) Y.-X. Lin, S.-N. Zhang, Z.-H. Xue, J.-J. Zhang, H. Su, T.-J. Zhao, G.-Y. Zhai, X.-H. Li, M. Antonietti, J.-S. Chen, *Nat. Commun.* **2019**, *10*, 4380.

- [17] H. Zhao, D. Zhang, H. Li, W. Qi, X. Wu, Y. Han, W. Cai, Z. Wang, J. Lai, L. Wang, *Adv. Energy Mater.* **2020**, *10*, 2002131.
- [18] H.-B. Wang, J.-Q. Wang, R. Zhang, C.-Q. Cheng, K.-W. Qiu, Y.-j. Yang, J. Mao, H. Liu, M. Du, C.-K. Dong, X.-W. Du, *ACS Catal.* **2020**, *10*, 4914.
- [19] a) E. Skulason, T. Bligaard, S. Gudmundsdóttir, F. Studt, J. Rossmeisl, F. Abild-Pedersen, T. Vegge, H. Jonsson, J. K. Nørskov, *Phys. Chem. Chem. Phys.* **2012**, *14*, 1235; b) B. Yu, H. Li, J. White, S. Donne, J. Yi, S. Xi, Y. Fu, G. Henkelman, H. Yu, Z. Chen, T. Ma, *Adv. Funct. Mater.* **2020**, *30*, 1905665.